Journal of Physics: Condensed Matter

PAPER

Magnetic field effect on trivial and topological bound states of superconducting quantum dot

To cite this article: G Górski *et al* 2020 *J. Phys.: Condens. Matter* **32** 445803

IOP Publishing Journal of Physics: Condensed Matter
J. Phys.: Condens. Matter **32** (2020) 445803 (11pp) https://doi.org/10.1088/1361-648X/aba38a

Magnetic field effect on trivial and topological bound states of superconducting quantum dot

G Górski[1,3], K Kucab[1] and T Domański[2]

[1] Institute of Physics, College of Natural Sciences, University of Rzeszów, ul. Pigonia 1, PL-35-310 Rzeszów, Poland
[2] Institute of Physics, M. Curie-Skłodowska University, ul. Radziszewskiego 10, PL-20-031 Lublin, Poland

E-mail: ggorski@ur.edu.pl

Received 12 May 2020, revised 2 July 2020
Accepted for publication 7 July 2020
Published 7 August 2020

Abstract

We investigate the properties of a quantum dot embedded between the normal and superconducting leads which is additionally side-attached to the topological superconducting nanowire, hosting the Majorana modes. This setup enables formation of the trivial (finite-energy) bound states induced in the quantum dot through the superconducting proximity effect, coexisting/competing with the topological (zero-energy) mode transmitted from the topological superconductor. We analyze their interplay, focusing on a role played by the external magnetic field. To distinguish between these bound states we analyze the qualitative and quantitative features manifested in the subgap charge tunneling originating under nonequilibrium conditions from the Andreev (particle to hole) scattering processes.

Keywords: Andreev scattering, bound states, superconducting proximity effect, Majorana quasiparticles

(Some figures may appear in colour only in the online journal)

1. Introduction

Due to the recent fast development of information techniques there is a growing need for novel devices, which could be alternative to the conventional semiconductor technology. One of promising routes in this pursuit is related to the quantum bits and quantum computations based on the quasiparticles, obeying non-abelian statistics [1–4]. Good candidates for such exotic quasiparticles are the Majorana zero-energy modes appearing at boundaries and/or defects in the topological superconductors [5, 6]. They can be regarded as mutations of the in-gap bound states [7] formed at the chemical potential which consist of the equal particle and hole ingredients, being thus identical to their own antiparticles [8–10]. Various implementations for realization of such Majorana quasiparticles have used the one-dimensional semiconducting (InSb or InAs) nanowires (NWs) characterized by the strong spin–orbit interaction [11–16] or nanochains of the selforganized magnetic atoms [17–21] proximitized to conventional *s*-wave superconductors. The superconducting (SC) proximity effect along with the spin–orbit interaction and the Zeeman field induce the intersite *p*-wave pairing of electrons. At some critical magnetic field ($B \sim 1$ T) it evolves to the topological phase, hosting the Majorana boundary modes.

Experimental tools for detecting these Majorana quasiparticles have predominantly relied on the charge transport measurements [11, 13, 15–19, 21, 22] looking for appearance of the zero-bias conductance peak (ZBCP) [23–25]. Similar zero-bias peak, however, can originate from other phenomena, such as disorder, critical field anisotropy, finite temperatures or the Kondo physics [26]. The latter effect has been thoroughly investigated, considering the correlated quantum dots (QDs) coupled either to the metallic contacts [27, 28] or embedded in the hybrid superconductor–semiconductor nanostructures [29–33]. In order to distinguish such ZBCP originating

[3] Author to whom any correspondence should be addressed.

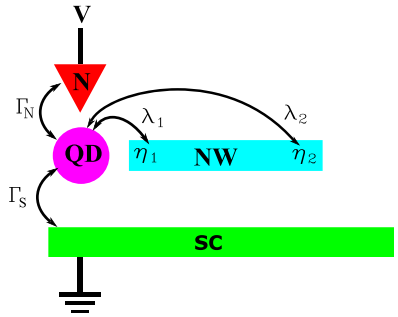

Figure 1. Scheme of a QD coupled to the normal (N) metallic tip and SC substrate which is additionally hybridized with the topological NW, hosting the Majorana modes η_1 and η_2.

from the Majorana bound states (MBS) from other effects (unrelated to the topological superconductivity) one hence needs the additionally supporting evidence.

In this regard, Liu and Baranger [34] have proposed to use the QD side-attached to the topological superconductor as a spectrometer of the Majorana features. In their setup the tunneling current flowing through the QD coupled to both metallic leads was predicted to exhibit the zero-bias conductance $e^2/2h$, originating from a fractional quantum interference with the Majorana mode. This characteristic value can be contrasted with the situations, when conventional fermion mode (transmitted e.g. from another QD whose energy level is near the chemical potential) would completely suppress the linear conductance down to zero [35–39]. Various hybrid configurations with the QDs attached to the topological NW have been investigated by a number of groups, considering the metallic [40–47] or ferromagnetic leads [48, 49].

We consider here a different geometry (figure 1), in which the QD is embedded into the Andreev-type tunneling setup and is side-coupled to the topological SC NW. The SC proximity effect induces the on-dot pairing whose consequences can be probed by the tunneling current driven by the bias V applied between the conducting and SC leads (we assume the superconductor to be grounded). For $|V|$ lower than the pairing energy gap Δ, the charge transport would be contributed solely by the Andreev (particle-to-hole) scattering processes [50]. In absence of the Majorana wire the optimal differential conductance of this setup would be $4e^2/h$, when the bias voltage is tuned to the energy of the bound state. Similar configurations with the Majorana wires have been previously addressed by several groups [51–54]. In particular, it has been predicted [52, 53] that a quantum interference caused by the MBS would reduce the differential conductance to e^2/h.

In this paper we study in detail the spectroscopic properties, inspecting their evolution against the magnetic field. Charge tunneling through the correlated QD coupled between the normal leads is usually characterized by the optimal differential conductance at zero magnetic field. In presence of the magnetic field the Kondo peak would split (through the Zeeman effect), suppressing the zero-bias conductance [55–57]. In contrast to such behavior, the magnetic field applied either to N–QD–SC or S–QD–S junctions affects the quasiparticle energies of the bound states [58]. Under specific conditions they can cross each other, giving rise to enhancement of the zero-bias conductance. By inspecting ZBCP as a function of magnetic field one can hence observe non-monotonous behavior [12, 29, 59, 60]. Experimental measurements for the hybrid system (shown in figure 1) revealed, that the optimal value of the ZBCP is stabilized over a broad range of the magnetic field [11, 13, 15, 61]. We analyze here such dependence of the Andreev current vs the magnetic field and show, that its differential conductance can be helpful for distinguishing the Majorana from the trivial quasiparticles.

The paper is organized as follows. In section 2 we formulate the microscopic model and present the formalism for determination of the subgap current. Next, we study the differential conductance of N–QD–S setup in absence of the MBS (section 3.1) and compare these results with the setup, in which the QD is coupled to the topological superconductor. In particular, we consider the limits of the long (section 3.2) and short (section 3.3) wire. In section 4 we summarize our results and in appendix A briefly discuss influence of the spin-polarized coupling between QD and NW.

2. The model and technique

We consider N–QD–SC junction with the topological SC wire attached to QD (figure 1). Our main objective is to study influence of the magnetic field on transport properties of this heterostructure. The effective low-energy scenario of the topological NW can be described by

$$H_{\mathrm{MQD}} = i\epsilon_m \eta_1 \eta_2 + \sum_{\alpha=1,2} \lambda_\alpha \left(\eta_\alpha d_\uparrow^\dagger + d_\uparrow \eta_\alpha \right), \qquad (1)$$

where $\eta_\alpha = \eta_\alpha^\dagger$ are the self-conjugated operators, ϵ_m stands for the overlap between MBSs, λ_α is the hybridization of α-MBS to the QD. As usually, $d_\sigma^\dagger(d_\sigma)$ denote the creation (annihilation) operators of the QD electron with spin σ. In the main part of this paper we assume the MBSs coupled only to $\sigma = \uparrow$ electrons. More general situation, taking into account the couplings to both spins, is considered in appendix A.

Our setup can be described by the Hamiltonian

$$H = H_{\mathrm{MQD}} + \sum_\sigma \epsilon_\sigma d_\sigma^\dagger d_\sigma + \sum_{\beta=\mathrm{S,N}} \left(H_\beta + H_{\beta-\mathrm{QD}} \right) \qquad (2)$$

where ϵ_σ is the spin-dependent QD energy. The Majorana modes usually emerge at some moderate magnetic field, on the order of 1 T. This affects the QD energy levels ϵ_σ, splitting them by the Zeeman energy $\epsilon_\downarrow - \epsilon_\uparrow = \mu_{\mathrm{B}} g B_0$ [62], where μ_{B} is the Bohr magneton and B_0 stands for the magnetic field.

The other contributions H_β appearing in (2) refer to the normal $\beta = \mathrm{N}$ and SC $\beta = \mathrm{S}$ leads, respectively. We describe the SC lead by the BCS-type Hamiltonian

$$H_{\mathrm{S}} = \sum_{\mathbf{k},\sigma} \xi_{\mathbf{k}\mathrm{S}} c_{\mathbf{k}\sigma\mathrm{S}}^\dagger c_{\mathbf{k}\sigma\mathrm{S}} - \sum_{\mathbf{k}} \left(\Delta c_{\mathbf{k}\uparrow\mathrm{S}}^\dagger c_{-\mathbf{k}\downarrow\mathrm{S}}^\dagger + \mathrm{h.c.} \right) \qquad (3)$$

with $c_{\mathbf{k}\sigma\mathrm{S}}^\dagger(c_{\mathbf{k}\sigma\mathrm{S}})$ being the creation (annihilation) operators of electrons whose energy $\xi_{\mathbf{k}\mathrm{S}} = \epsilon_{\mathbf{k}\mathrm{S}} - \mu_{\mathrm{S}}$ is measured from the chemical potential μ_{S}. We treat this chemical potential as a

convenient reference level for all energies ($\mu_S \equiv 0$). The pairing gap Δ depends on the magnetic field. Following [30], we choose

$$\Delta = \Delta_0\sqrt{1-(B/B_{cr})^2}, \tag{4}$$

where B_{cr} is the critical field at which the gap closes. The normal electrode is treated as a free fermion gas

$$H_N = \sum_{\mathbf{k},\sigma}\xi_{\mathbf{k}N}c^\dagger_{\mathbf{k}\sigma N}c_{\mathbf{k}\sigma N}, \tag{5}$$

where $c^\dagger_{\mathbf{k}\sigma N}(c_{\mathbf{k}\sigma N})$ denote the creation (annihilation) operators of electron with momentum $\mathbf{k}$ and spin σ whose energy $\xi_{\mathbf{k}N} = \epsilon_{\mathbf{k}N} - \mu_N$ is measured with respect to the chemical potential μ_N. Applying the bias voltage V one can lift/lower this chemical potential $\mu_N = eV$. Couplings of the QD to both external reservoirs is expressed by the hybridization term

$$H_{\beta-QD} = \sum_{\mathbf{k},\sigma}(V_{\mathbf{k}\beta}d^\dagger_\sigma c_{\mathbf{k}\sigma\beta} + \text{h.c.}) \tag{6}$$

with the matrix elements $V_{\mathbf{k}\beta}$. We introduce the auxiliary couplings $\Gamma_\beta = 2\pi\sum_{\mathbf{k}}|V_{\mathbf{k}\beta}|^2\delta(\omega-\xi_{\mathbf{k}\beta})$, assuming them to be constant in the subgap regime.

For convenience, we replace $\eta_{1,2}$ by the standard fermion operators [9] $\eta_1 = \frac{1}{\sqrt{2}}(f+f^\dagger)$, $\eta_2 = \frac{i}{\sqrt{2}}(f^\dagger - f)$ and represent the couplings λ_α of QD to the Majorana modes as $\lambda_1 = \sqrt{2}t_{m1}$ and $\lambda_2 = i\sqrt{2}t_{m2}$, respectively. Equation (1) simplifies then to the following structure [45]

$$H_{MQD} = \epsilon_m\left(f^\dagger f - \frac{1}{2}\right) + t_+\left(d^\dagger_\uparrow f - d_\uparrow f^\dagger\right) + t_-\left(d^\dagger_\uparrow f^\dagger - d_\uparrow f\right), \tag{7}$$

where $t_+ = t_{m1} + t_{m2}$ and $t_- = t_{m1} - t_{m2}$.

2.1. Method

The spectral and transport properties of our system can be determined within the Green's function approach. The SC proximity effect can be taken into account, using the Nambu representation augmented with the fermionic degrees of freedom related to the MBSs $\Psi = (d_\uparrow, d^\dagger_\uparrow, d_\downarrow, d^\dagger_\downarrow, f, f^\dagger)$. For this purpose we consider the retarded spin-Nambu Green's function $\mathcal{G}(t) = -i\theta(t)\langle\Psi(t)\Psi^\dagger(0) + \Psi^\dagger(0)\Psi(t)\rangle$, where $\theta(t)$ is the step function, $\langle\ldots\rangle$ denotes the statistical averaging, and the time-dependent operators are defined as $\Psi(t) = e^{itH/\hbar}\Psi e^{-itH/\hbar}$. Fourier transform of $\mathcal{G}(t)$ takes the following form

$$\mathcal{G}^{-1}(\omega) = \begin{pmatrix} \omega-\epsilon_\uparrow-\Sigma_0(\omega) & 0 & 0 & -\Sigma_1(\omega) & -t_+ & -t_- \\ 0 & \omega+\epsilon_\uparrow-\Sigma_0(\omega) & \Sigma_1^*(-\omega) & 0 & t_- & t_+ \\ 0 & \Sigma_1^*(-\omega) & \omega-\epsilon_\downarrow-\Sigma_0(\omega) & 0 & 0 & 0 \\ -\Sigma_1(\omega) & 0 & 0 & \omega+\epsilon_\downarrow-\Sigma_0(\omega) & 0 & 0 \\ -t_+ & t_- & 0 & 0 & \omega-\epsilon_m & 0 \\ -t_- & t_+ & 0 & 0 & 0 & \omega+\epsilon_m \end{pmatrix}, \tag{8}$$

where the selfenergy terms are given by [63]

$$\Sigma_0(\omega) = -i\frac{\Gamma_N}{2} - \frac{\Gamma_S}{2}\varphi(\omega), \tag{9}$$

$$\Sigma_1(\omega) = -\frac{\Gamma_S}{2}\frac{\Delta}{\omega}\varphi(\omega) \tag{10}$$

and

$$\varphi(\omega) = \begin{cases} \dfrac{|\omega|}{\sqrt{\omega^2-\Delta^2}} & \text{for } |\omega| > \Delta, \\ -i\dfrac{\omega}{\sqrt{\Delta^2-\omega^2}} & \text{for } |\omega| < \Delta. \end{cases} \tag{11}$$

2.2. Tunneling current

The charge current, $I_T = \sum_\sigma\left(I^\sigma_A + I^\sigma_Q\right)$, induced through N–QD–SC heterojunction by the voltage V consists of the Andreev I^σ_A and the quasi-particle contributions I^σ_Q, respectively. Within the Landauer-type approach they can be expressed as [63, 64]

$$I^\sigma_A = \frac{2e}{h}\int T^\sigma_A(\omega)\left[f(\omega-eV) - f(\omega+eV)\right]d\omega, \tag{12}$$

$$I^\sigma_Q = \frac{2e}{h}\int T^\sigma_Q(\omega)\left[f(\omega-eV) - f(\omega)\right]d\omega, \tag{13}$$

where $f(\omega) = \left[1+\exp\left(\omega/k_BT\right)\right]^{-1}$ denotes the Fermi–Dirac distribution function. The spin-resolved Andreev transmittance is given by

$$T^\uparrow_A(\omega) = |\Gamma_N|^2|\mathcal{G}_{14}(\omega)|^2, \tag{14}$$

$$T^\downarrow_A(\omega) = |\Gamma_N|^2|\mathcal{G}_{23}(\omega)|^2 \tag{15}$$

and the quasi-particle transmittance is

$$T^\uparrow_Q(\omega) = \Gamma_N\Gamma_S\ \text{Re}[\varphi(\omega)] \times\left[|\mathcal{G}_{11}(\omega)|^2 + |\mathcal{G}_{14}(\omega)|^2 - \frac{2\Delta}{\omega}\text{Re}\left[\mathcal{G}_{11}(\omega)\mathcal{G}^*_{14}(\omega)\right]\right] \tag{16}$$

$$T^\downarrow_Q(\omega) = \Gamma_N\Gamma_S\ \text{Re}[\varphi(\omega)] \times\left[|\mathcal{G}_{33}(\omega)|^2 + |\mathcal{G}_{23}(\omega)|^2 + \frac{2\Delta}{\omega}\text{Re}\left[\mathcal{G}_{33}(\omega)\mathcal{G}^*_{23}(\omega)\right]\right]. \tag{17}$$

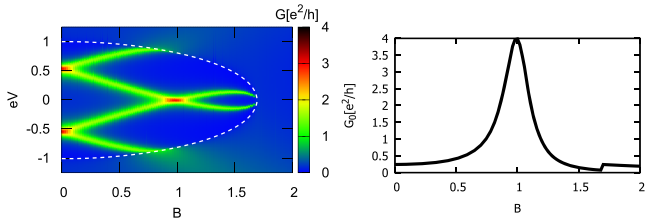

Figure 2. Left panel: the differential conductance $G = \mathrm{d}I/\mathrm{d}V$ as a function of the bias voltage V and magnetic field B for $\Gamma_S = 2$, $\Gamma_N = 0.25$ and $t_{m1} = 0$. Right panel: dependence of the zero-bias conductance $G_0 = G(0)$ on magnetic field.

The Andreev current occurs when electron arriving from the normal lead is converted (on QD) into the pair and next propagates to the SC electrode, while simultaneously a hole with opposite spin is reflected back to the normal lead. Contributions of the Andreev current, I_A, and the quasi-particle current, I_Q^σ, to the total charge transport are sensitive to the ratio $|eV|/\Delta$. For $|eV| < \Delta$ the quasi-particle current vanishes $I_Q^\sigma = 0$, therefore the subgap transport is contributed solely by the Andreev refection mechanism. For $|eV| > \Delta$ the dominant contribution comes from the quasi-particle current, I_Q^σ, and for increasing $|V|$ the particle–hole reflections become less and less efficient [65].

3. The numerical results

In this section we analyze the differential conductance $G = \mathrm{d}I/\mathrm{d}V$ of the tunneling current $I = \sum_\sigma \left(I_A^\sigma + I_Q^\sigma\right)$, focusing on its variation with respect to the magnetic field. Hybridization of the QD with any SC reservoir induces the electron pairing, leading to formation of the in-gap bound states symmetrically around the chemical potential μ_S. Since the magnetic field splits the QD level $\epsilon_\downarrow \neq \epsilon_\uparrow$ this is going to affect the in-gap states and shall be manifested in the sub-gap conductance [12, 29, 59, 60]. In particular, such bound states can also cross each other, undergoing the quantum phase transition [66].

In the present hybrid structure, comprising the side-attached topological superconductor, there is also a possibility of the Majorana quasiparticle leakage onto the QD. This has been indeed evidenced empirically by the ZBCP [11, 13, 15, 16, 22, 60, 67] in the tunneling measurements. In what follows, we show the numerical results obtained for N–QD–SC heterostructure, considering the trivial case $\lambda_\alpha = 0$ (section 3.1) and the same heterostructure with the QD coupled to the long (section 3.2) and short (section 3.3) topological NWs, respectively.

We choose for computations the zero-temperature pairing gap as the energy unit ($\Delta_0 = 1$). Our studies are done for the strong coupling to SC lead ($\Gamma_S = 2$), assuming the weak coupling to the normal N electrode ($\Gamma_N = 0.25$) because otherwise the quasiparticle broadening would smear the in-gap features. The critical field, B_{cr}, at which the SC gap closes is imposed as $B_{cr} = 1.7\Delta_0$.

3.1. Magnetic field effect on trivial states

Let us consider first the magnetic field dependent transport properties of N–QD–SC heterostructure in absence of the Majorana fermions ($t_{m1,m2} = 0$) [29, 64]. Coupling of the QD to the SC lead induces the on-dot pairing, which is manifested by the gaped density of states and emergence of the in-gap bound states. Energies of these trivial bound states depend on ϵ_σ, Δ, and Γ_S. In the limit $\Gamma_N \to 0$ such bound states appear at $z\left(\pm\frac{\epsilon_\uparrow - \epsilon_\downarrow}{2} \pm \frac{1}{2}\sqrt{(\epsilon_\uparrow + \epsilon_\downarrow)^2 + \Gamma_S^2}\right)$ where $z = (1 + \frac{\Gamma_S}{2\Delta})^{-1}$ is quasiparticle weight factor [68, 69]. Their positions can be observed experimentally by enhancement of the subgap conductance [29, 60, 70–73].

The external magnetic field splits these Andreev peaks [29, 59, 60, 64] because of the spin-dependent QD level $\epsilon_{\uparrow,\downarrow} = \epsilon \pm B$, where $B = \frac{1}{2}g\mu_B B_0$. In consequence, we observe appearance of four bound states. A pair of the inner bound states eventually cross each other, when $B \approx \Gamma_S/2$. Figure 2 displays the differential conductance $G = \mathrm{d}I/\mathrm{d}V$ versus the bias voltage V and the magnetic field B obtained for $\epsilon = 0$. The white dashed line refers to $eV = \Delta(B)$ and denotes a boundary between the pure subgap Andreev conductance G_A with another region, where the quasi-particle conductance G_Q is finite. We notice, that by increasing the magnetic field the outer bound states merge with a continuum region, while the inner bound states reveal the aforementioned crossing at $B \approx \Gamma_S/2$. At this particular magnetic field we observe, that the zero-bias conductance approaches the optimal value equal to $4e^2/h$ (see the right panel in figure 2). Further increase of the magnetic field separates these bound states, therefore the zero-bias conductance is suppressed. At the critical magnetic field ($B_{cr} \approx 1.7$) the SC gap closes. For this reason at higher magnetic fields the conductance originates entirely from the quasi-particle tunneling [65]. Such changeover is manifested by a tiny discontinuity of the linear conductance G_0, when approaching $B \to B_{cr}$.

Figure 3 presents the differential conductance with respect to the bias voltage V and the QD level ϵ (which can be varied by the gate potential) obtained for several values of the magnetic field, as indicated. At $B = 0$ we observe only one pair of the bound states with the optimal conductance appearing at finite voltage. For the weak magnetic field there are four branches of the in-gap bound states. At the critical magnetic field $B = \Gamma_S/2$ a pair of the inner bound states overlap with one another. At the stronger magnetic field the inner pair of bound states takes a form of the loop structure, whereas the outer bound states merge with a continuum (where they are hardly visible). Similar qualitative behavior has been observed experimentally by Deng *et al* [13] and by other groups [12, 29].

3.2. QD coupled to a long topological wire

The spectroscopic properties of N–QD–SC heterojunction substantially change when the QD is coupled to the Majorana mode(s) [51–53, 74]. To inspect the role of magnetic field, let us first consider the long topological SC wire, where the Majorana modes do not overlap with one another ($\epsilon_m = 0$) and only η_1 is directly hybridized with the QD, $t_{m2} = 0$. Under such

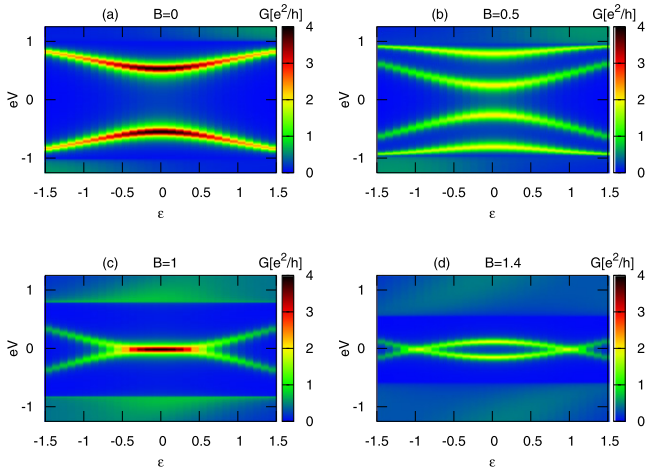

Figure 3. The differential conductance $G = \mathrm{d}I/\mathrm{d}V$ of the tunneling current flowing though N–QD–S heterostructure as a function of the bias voltage V and the QD energy ϵ obtained for different values of the magnetic field, as indicated. We used the model parameters $\Gamma_S = 2$ and $\Gamma_N = 0.25$.

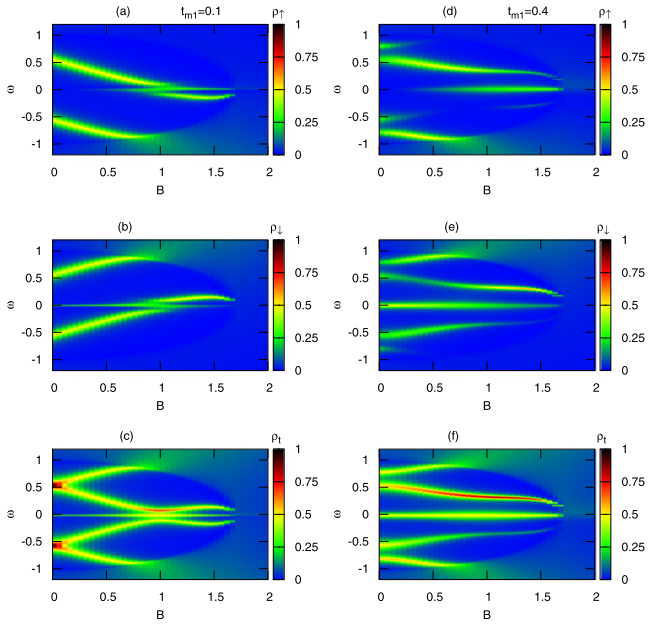

Figure 4. The spin-resolved spectral function $\rho_\sigma(\omega)$ and total spectral function $\rho_t(\omega)$ varying with respect to the magnetic field obtained for the weak $t_{m1} = 0.1$ (left) and strong coupling $t_{m1} = 0.4$ (right), respectively. We used the model parameters $\epsilon = 0$, $\Gamma_S = 2$, $\Gamma_N = 0.25$, $\epsilon_m = 0$.

conditions the spectrum of QD reveals some novel features, displayed in figure 4.

In absence of the magnetic field we have previously shown [53], that the matrix Green's function (8) is characterized by five poles. One of them corresponds to the zero-energy Majorana mode transmitted onto QD from the NW and the other ones appearing at $\pm z\sqrt{C \pm \frac{1}{2}\sqrt{D}}$, where $C = \frac{\epsilon_\uparrow^2+\epsilon_\downarrow^2}{2} + \Gamma_S^2/4 + 2t_{m1}^2$ and $D = (\epsilon_\uparrow^2 - \epsilon_\downarrow^2 + 4t_{m1}^2)^2 + \Gamma_S^2(\epsilon_\uparrow - \epsilon_\downarrow)^2$, represent the trivial bound states which are partly affected by the Majorana mode. Such five-pole structure is particularly evident in the strong coupling ($t_{m1} > \Gamma_N$) limit (right side panels in figure 4). The spin resolved spectra reveal differences, mainly in the spectral weights of the trivial bound states. In both spin sectors, however, we clearly observe the common *avoided crossing* behavior whenever the trivial bound states approach the zero-energy mode. Spectral weight of the zero-energy mode depends on the spin sector as well. Physically this effect comes from the direct (indirect) coupling of the topological NW to ↑ (↓) electrons.

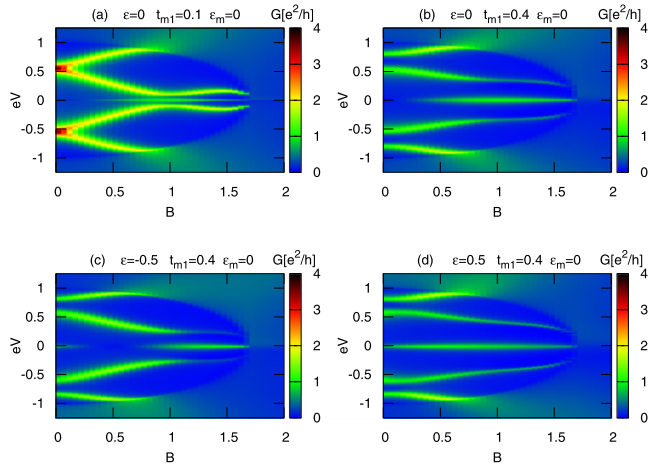

Figure 5. Variation of the differential conductance G with respect to magnetic field B and bias voltage V obtained for $\epsilon_m = 0$, $\Gamma_S = 2$, $\Gamma_N = 0.25$ and (a) $t_{m1} = 0.1$, $\epsilon = 0$; (b) $t_{m1} = 0.4$, $\epsilon = 0$; (c) $t_{m1} = 0.4$, $\epsilon = -0.5$; (d) $t_{m1} = 0.4$, $\epsilon = 0.5$.

At $B = 0$ the spectrum of ↑ electrons (which is directly coupled to the Majorana mode) is characterized by four peaks and a dip at $\omega = 0$, where the density is reduced by half in comparison to the system without the Majorana wire, $\rho_\uparrow(0)_{t_{m1}\neq 0} = 0.5\rho_\uparrow(0)_{t_{m1}=0}$. This reduction of the spectral function $\rho_\uparrow(\omega = 0)$ is caused by a partial leakage of ↑ electrons onto the topological NW.

Influence of the Majorana quasiparticle is also well manifested in the differential conductance of our heterostructure. Figure 5 presents $G(V) = \mathrm{d}I/\mathrm{d}V$ versus the magnetic field B and the bias voltage V. In the strong coupling t_{m1} limit (panel (b)) we clearly notice a considerable separation of the trivial bound states from the Majorana mode. Upon increasing the magnetic field the trivial bound states change their energies: the outer ones merge with a continuum region whereas the inner ones approach each other and gradually loose their spectral weights at expense of the enhanced ZBCP. Such behavior can be contrasted with N–QD–SC heterostructure (figure 2), where the ZBCP is driven solely from a crossing of the trivial bound states. This avoided-crossing tendency between the trivial and topological bound states have been indeed observed in presence of the magnetic field by the Copenhagen group [16].

The bottom panels in figure 5 show the tunneling conductance $\mathrm{d}I/\mathrm{d}V$ obtained for non-zero energy level of the QD ($\epsilon \neq 0$), which could be realized by applying the gate potential. ZBCP turns out to be sensitive, both to the magnetic field B and the QD energy level ϵ. The optimal conditions for such zero-bias conductance $G(0)$ are presented in figure 6. Let us

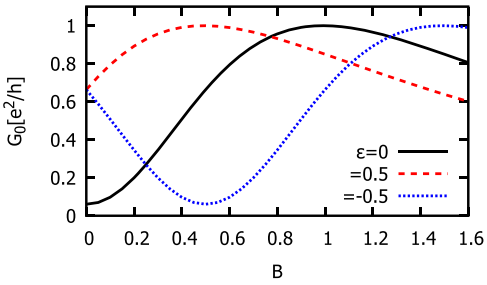

Figure 6. The zero-bias conductance as a function of the magnetic field for several values of the QD energy level $\epsilon = 0$ (solid line), $\epsilon = 0.5$ (dashed line) and $\epsilon = -0.5$ (dotted line). Results are obtained for the model parameters $\Gamma_S = 2$, $\Gamma_N = 0.25$, $\epsilon_m = 0$, $t_{m1} = 0.4$.

remark, that for arbitrary ϵ the optimal value of the zero-bias conductance approaches e^2/h, being four-fold smaller than $G(V=0)_{t_{m1}=0}$ in absence of the Majorana quasiparticles (see the right panel in figure 2). This feature stems from a fractional character of the Majorana mode, interfering with the QD.

3.3. QD coupled to a short topological wire

The separated Majorana modes are pretty robust against the perturbations from an environment, owing to their topological protection. Any overlap, however, between the Majorana quasiparticles $\epsilon_m \neq 0$ or finite coupling $t_{m2} \neq 0$ can spoil this protection, inducing some novel spectroscopic features differing from the zero-energy quasiparticles [15, 33, 75–78]. For the QD–topological SC wire hybrid structures Clarke [76] has introduced the useful concept of *topological quality factor* $q = 1 - \frac{t_{m2}}{t_{m1}}$ and emphasized that non-abelian properties would be preserved only when $q \approx 1$.

Figure 7 displays the influence of t_{m2} coupling on the differential conductance $G(V)$ obtained for $\epsilon_m = 0$. In comparison to the case $t_{m2} = 0$ (figure 5) we notice the splitting of the zero-bias peak into two (lower and upper) branches. In particular, for $t_{m2} = t_{m1}$ (panel (b) in figure 7) these branches ultimately merge with the trivial bound states at some value of the magnetic field (here for $B \approx 1.1$), where the differential conductance is locally enhanced. Similar behavior has been previously predicted theoretically by Prada *et al* [75] for the topological NW hybridized with N–QD–N junctions. For all values of the magnetic field the zero-bias conductance practically vanishes $G(V=0) \approx 0$, what can be interpreted as a result of the complete destructive quantum interference. For a comparison let us recall, that for $t_{m1} \neq 0$ and $t_{m2} = 0$ the linear conductance is reduced only by factor $1/4$ [53].

Finally let us explore influence of the magnetic field on the transport properties of N–QD–SC setup, assuming the topological NW to be short enough to guarantee an overlap between the Majorana quasiparticles $\epsilon_m \neq 0$. Under such circumstances the leaking Majorana modes induces two resonances appearing in the QD spectral function. For $B = 0$ they occur at $\omega = \pm\epsilon_m$ [15, 52, 75, 79]. The magnetic field strongly affects these features. Figure 8(a) presents the differential conductance as a function of the bias voltage V and the magnetic field B

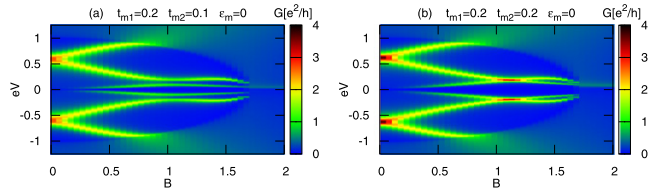

Figure 7. The differential conductance dI/dV as a function of the bias voltage V and the magnetic field B obtained for different values of t_{m2}. Other parameters $\epsilon = 0$, $\Gamma_S = 2$, $\Gamma_N = 0.25$, $t_{m1} = 0.2$ and $\epsilon_m = 0$.

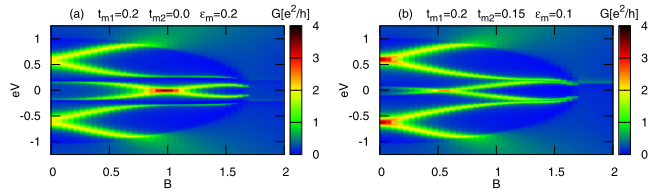

Figure 8. The differential conductance dI/dV as a function of the bias voltage V and the magnetic field B obtained for $t_{m2} = 0$, $\epsilon_m = 0.2$ (a) and $t_{m2} = 0.15$, $\epsilon_m = 0.1$ (b). Other parameters $\epsilon = 0$, $\Gamma_S = 2$, $\Gamma_N = 0.25$ and $t_{m1} = 0.2$.

obtained for $\epsilon_m = 0.2$ and $t_{m2} = 0$ for the same set of model parameters as in the previous sections. Upon increasing the magnetic field we again notice a splitting of the trivial bound states. The inner states gradually move towards each other and near $eV \approx \pm\epsilon_m$ they show an anti-crossing tendency from the low-energy (Majorana) features. At the characteristic magnetic field (here $B \approx \Gamma_S/2$) these low-energy features eventually cross each other, enhancing the zero-bias conductance up to $4e^2/h$. This effect is in stark contrast with the properties of similar setup obtained for $\varepsilon_m = 0$ (discussed in section 3.2). This zero-bias conductance is reminiscent of the conventional N–QD–SC heterojunction in absence of any topological SC wire.

For the case $t_{m2} \neq 0$, $|\epsilon_m| < t_{m2}$ (see panel (b) in figure 8) we observe, that spectroscopic properties vary qualitatively against the magnetic field. In the limit of weak magnetic field the signatures of Majorana modes are induced nearby the zero energy (like for finite ϵ_m and $t_{m2} = 0$ as shown in figure 8(a)). Contrary to that, for the strong magnetic field we again notice the well pronounced splitting between the lower and upper Majorana-branches, similar to the case $\epsilon_m = 0$ and finite t_{m2} presented in figure 7.

3.4. Influence of QD level

All qualitative properties discussed so far for the long (section 3.2) and short (section 3.3) NWs are also observed, when considering the influence of QD energy level. In practice ϵ could be experimentally varied by applying the gate potentials. Figure 9 shows the anti-crossing behavior observable in the tunneling conductance against the energy level ϵ which occurs near $\epsilon \approx \pm B$. In distinction to the system without the Majorana quasiparticles (figure 3) the tunneling conductance is asymmetric with respect to ϵ. Such characteristic

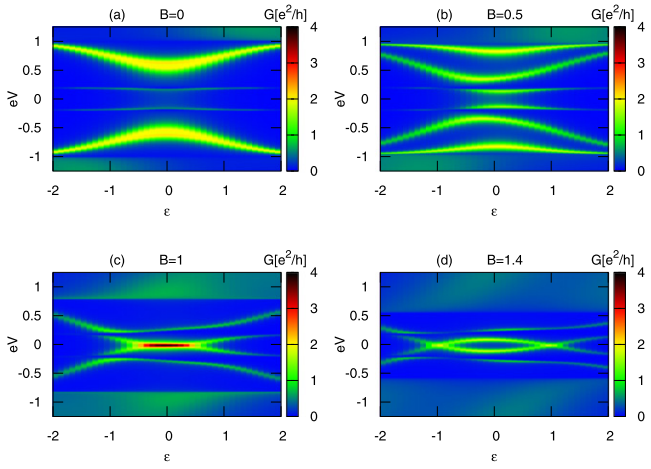

Figure 9. Variation of the differential conductance $\mathrm{d}I/\mathrm{d}V$ with respect to the bias voltage V and the QD energy level ϵ obtained for several magnetic fields (as indicated) using the model parameters $\Gamma_S = 2$, $\Gamma_N = 0.25$, $t_{m1} = 0.2$, $t_{m2} = 0$ and $\epsilon_m = 0.2$.

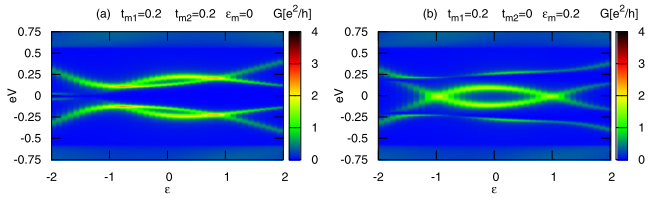

Figure 10. Variation of the differential conductance $\mathrm{d}I/\mathrm{d}V$ with respect to the bias voltage V and the QD energy level ϵ obtained for $\epsilon_m = 0$ and $t_{m2} = 0.2$ (a) or $\epsilon_m = 0.2$ and $t_{m2} = 0$ (b). Other parameters $\Gamma_S = 2$, $\Gamma_N = 0.25$, $t_{m1} = 0.2$ and $B = 1.4$.

dependence of $G(V, \epsilon)$ has been reported experimentally by Copenhagen [13] and Delft [60] groups. Prada *et al* [75] analyzed the low-energy QD spectrum, taking into account the couplings to both Majorana modes ($t_{m1,m2} \neq 0$) and considering their overlap ($\epsilon_m \neq 0$). Under such circumstances the QD spectrum develops the characteristic *bow-tie* shape, especially in the limit $t_{m2} \ll (t_{m1}, \epsilon_m)$. In our case this *bow-tie structure* is appearing at sufficiently large magnetic field $B > \Gamma_S/2$ (figure 9(d)).

Figure 10 presents the differential conductance with respect the QD energy level ϵ. We focus on two extreme situations, corresponding to: (i) the identical couplings of QD to both MBS $t_{m1} = t_{m2}$ without any overlap $\epsilon_m = 0$, and (ii) the finite coupling of QD only to the left-side MBS, assuming $t_{m1} = \epsilon_m$. In the first case we observe that, the trivial bound states merge with the Majorana feature. This resembles the *diamond* structure predicted by Prada *et al* [75] and Clarke [76]. In the second case we notice the crossings of Majorana features, acquiring the characteristic *bow-tie* form [75].

4. Conclusions

We have theoretically studied the charge transport through the normal metal–quantum dot–superconductor (N–QD–SC) heterojunction, where QD is side-coupled to the topological SC wire. We have investigated a role played by the magnetic field, which (a) splits the QD level by the Zeeman energy and (b) affects the energy gap of SC lead $\Delta(B)$. We have shown, that the charge tunneling contributed by the Andreev-type scattering mechanism could be useful to distinguish the Majorana features leaking onto the QD from its trivial bound states. The characteristic Majorana signatures would be observable, both in the line-shapes of the differential conductance and in the magnitude of its zero-bias value.

In the case, when QD is coupled to the long topological SC wire (without any overlap between the Majorana modes) the zero-bias conductance would reach the optimal value equal to e^2/h. This feature stems from a fractional character of the Majorana quasiparticle. Our calculations show, that a pronounced ZBPC would persist over a broad range of the magnetic field. This behavior is in stark contrast to the properties of N–QD–SC heterostructures in absence of the topological SC wire, where a crossing of the trivial bound states (at some magnetic field and/or QD level) could enhance the zero-bias conductance to the maximal value $4e^2/h$, corresponding to the perfect Andreev conductance [33]. For the QD coupled to the short topological SC wire (where the Majorana modes overlap with one another $\epsilon_m \neq 0$) we obtain the zero-bias conductance analogous to the conventional N–QD–SC heterostructure. Fingerprints of the overlapping Majorana quasiparticles are also evidenced in the voltage-dependent differential conductance by the anti-crossing behavior, appearing at $V \approx \pm\epsilon_m/e$. Influence of the magnetic field on the spectroscopic properties of N–QD–S heterostructure attached to the topological SC NW could be thus useful for detecting the Majorana mode(s).

In future studies it would be worth to consider the correlation effects driven by the Coulomb repulsion between the opposite spin electrons in order to check the role of the Kondo effect. In presence of the magnetic field its signatures are expected to appear away from the zero-bias conductance, they should be hence distinguishable from the Majorana features.

Acknowledgments

This project is supported by National Science Centre (NCN, Poland) under the Grants 2017/27/B/ST3/01911 (TD) and 2018/29/B/ST3/00937 (GG).

Conflict of interest

The authors declare no conflicts of interest.

Appendix A. Spin-dependent tunneling between QD and topological wire

Influence of the spin-dependent tunneling between the QD and Majorana wire on the spectral properties has been partly investigated, considering both N–QD–N [15, 75, 80–83] and N–QD–SC [74] heterostructures. For N–QD–N junctions we have previously shown [83], that this spin-dependent tunneling affects the polarization of transport properties,

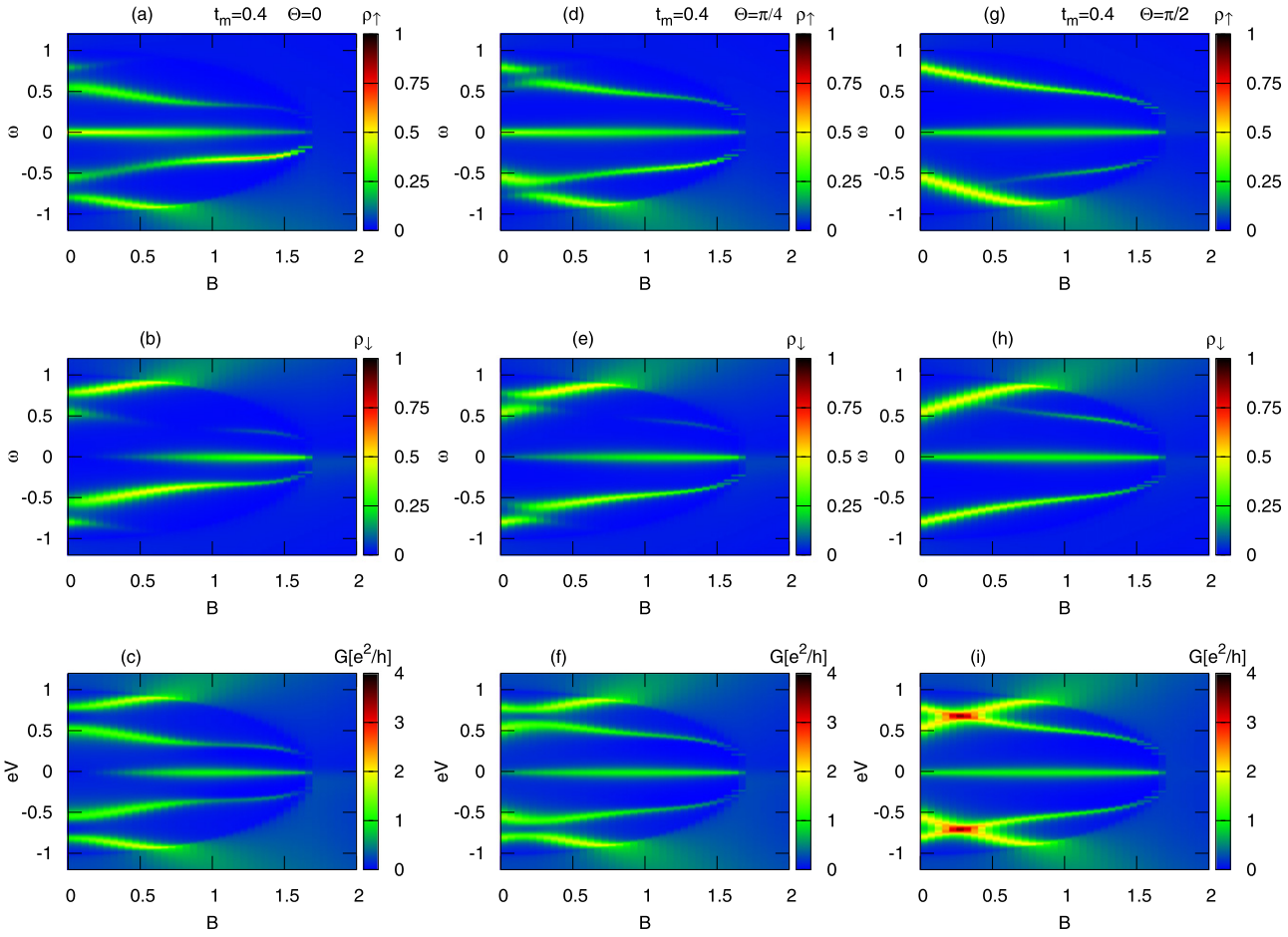

Figure A1. The spin-dependent spectral functions, $\rho_\sigma(\omega)$ (top and middle panels), and the differential tunneling conductance, $G(V)$ (bottom panels), as the functions of magnetic field B obtained for several values of the canting angle θ assuming the model parameters $\epsilon = 0$, $\Gamma_S = 2$, $\Gamma_N = 0.25$, $\epsilon_m = 0$, $t_{m1} = 0.4$ and $t_{m2} = 0$.

such as the spin-dependent zero-bias conductance and spin-dependent thermopower, while the total (finite-bias) transport properties are rather very weakly dependent on the polarization of tunneling amplitudes. In this appendix we briefly inspect the effect of spin-polarized coupling on properties N–QD–SC heterostructure in presence of the magnetic field.

We can describe our setup with such spin-dependent tunneling amplitude using the Hamiltonian

$$H = \sum_\sigma t_\sigma \left(d_\sigma^\dagger - d_\sigma\right)\left(f + f^\dagger\right) + \epsilon_m\left(f^\dagger f - \frac{1}{2}\right) + \sum_\sigma \epsilon_\sigma d_\sigma^\dagger d_\sigma + \sum_{\beta=\mathrm{S,N}}\left(H_\beta + H_{\beta-\mathrm{QD}}\right), \tag{A.1}$$

where $t_\sigma = \lambda_{1\sigma}/\sqrt{2}$. The retarded Green's function defined in the spin-Nambu representation takes the following form

$$\mathcal{G}^{-1}(\omega) = \begin{pmatrix} \omega - \epsilon_\uparrow - \Sigma_0(\omega) & 0 & 0 & -\Sigma_1(\omega) & -t_\uparrow & -t_\uparrow \\ 0 & \omega + \epsilon_\uparrow - \Sigma_0(\omega) & \Sigma_1^*(-\omega) & 0 & t_\uparrow & t_\uparrow \\ 0 & \Sigma_1^*(-\omega) & \omega - \epsilon_\downarrow - \Sigma_0(\omega) & 0 & -t_\downarrow & -t_\downarrow \\ -\Sigma_1(\omega) & 0 & 0 & \omega + \epsilon_\downarrow - \Sigma_0(\omega) & t_\downarrow & t_\downarrow \\ -t_\uparrow & t_\uparrow & -t_\downarrow & t_\downarrow & \omega - \epsilon_m & 0 \\ -t_\uparrow & t_\uparrow & -t_\downarrow & t_\downarrow & 0 & \omega + \epsilon_m \end{pmatrix}. \tag{A.2}$$

Prada *et al* [75] has proposed to represent the spin-dependent hopping amplitudes t_σ

$$t_\uparrow = t_{m1} \sin\left(\frac{\theta}{2}\right) \tag{A.3}$$

$$t_\downarrow = -t_{m1} \cos\left(\frac{\theta}{2}\right) \tag{A.4}$$

in terms of the auxiliary *canting* angle θ of the first Majorana mode. This canting angle can vary in the range $0 \leqslant \theta \leqslant \pi$ [15].

In figure A1 we show the spin-dependent spectral functions, ρ_σ, and the differential tunneling conductance, $G(V)$, obtained for a few representative values of the canting angle θ. Panels (a)–(c) present the results for $\theta = \pi$, corresponding to the strong polarization of the hopping amplitude ($t_\uparrow = t_{m1}$ and $t_\downarrow = 0$). In this case the signatures of the zero-energy Majorana mode show up in the spectral function $\rho_\uparrow$ at some finite magnetic field, whereas the zero-energy peak exists in $\rho_\downarrow$ for all values of the magnetic field. Because of the particle–hole Andreev scattering mechanism the ZBCP can emerge at this finite magnetic field. In panels (d)–(f) we use $\theta = 3\pi/4$, which corresponds to $|t_\uparrow| > |t_\downarrow|$ and in panels (g)–(i) we use $\theta = \pi/2$, referring to $|t_\uparrow| = |t_\downarrow|$. For the finite values of both spin-dependent hopping amplitudes we observe enhancement of the spectral weight of the Majorana mode appearing in $\rho_\uparrow$. Furthermore, the ZBCP is present starting from the zero magnetic field.

We thus conclude, that the finite hopping amplitude in both spin sectors is responsible for shifting the zero-bias conductance to somewhat smaller magnetic fields, leaving its optimal value $G_0 = e^2/h$ untouched. For the large bias voltages $|V|$ we also observe possible crossings of the trivial bound states, giving rise to the enhanced differential conductance.

ORCID iDs

G Górski https://orcid.org/0000-0003-2880-5524
K Kucab https://orcid.org/0000-0001-6157-3775
T Domański https://orcid.org/0000-0003-1977-3989

References

[1] Nayak C, Simon S H, Stern A, Freedman M and Das Sarma S 2008 Non-abelian anyons and topological quantum computation *Rev. Mod. Phys.* **80** 1083
[2] Tewari S, Das Sarma S, Nayak C, Zhang C and Zoller P 2007 Quantum computation using vortices and Majorana zero modes of a $p_x + ip_y$ superfluid of fermionic cold atoms *Phys. Rev. Lett.* **98** 010506
[3] Kitaev A Y 2001 Unpaired Majorana fermions in quantum wires *Phys. Usp.* **44** 131
[4] Kitaev A Y 2003 Fault-tolerant quantum computation by anyons *Ann. Phys.* **303** 2
[5] Das Sarma S, Freedman M and Nayak C 2015 Majorana zero modes and topological quantum computation *npj Quantum Inf.* **1** 15001
[6] Lutchyn R M, Bakkers E P A M, Kouwenhoven L P, Krogstrup P, Marcus C M and Oreg Y 2018 Majorana zero modes in superconductor–semiconductor heterostructures *Nat. Rev. Mater.* **3** 52
[7] Chevallier D, Simon P and Bena C Oct 2013 From Andreev bound states to Majorana fermions in topological wires on superconducting substrates: a story of mutation *Phys. Rev.* B **88** 165401
[8] Alicea J 2012 New directions in the pursuit of Majorana fermions in solid state systems *Rep. Prog. Phys.* **75** 076501
[9] Elliott S R and Franz M Feb 2015 Colloquium: Majorana fermions in nuclear, particle, and solid-state physics *Rev. Mod. Phys.* **87** 137
[10] Aguado R 2017 Majorana quasiparticles in condensed matter *Riv. Nuovo Cimento* **040** 523
[11] Mourik V, Zuo K, Frolov S M, Plissard S R, Bakkers E P A M and Kouwenhoven L P 2012 Signatures of Majorana fermions in hybrid superconductor–semiconductor nanowire devices *Science* **336** 1003
[12] Das A, Ronen Y, Most Y, Oreg Y, Heiblum M and Shtrikman H 2012 Zero-bias peaks and splitting in an Al–InAs nanowire topological superconductor as a signature of Majorana fermions *Nat. Phys.* **8** 887
[13] Deng M T, Vaitiekėnas S, Hansen E B, Danon J, Leijnse M, Flensberg K, Nygård J, Krogstrup P and Marcus C M 2016 Majorana bound state in a coupled quantum-dot hybrid-nanowire system *Science* **354** 1557
[14] Albrecht S M, Higginbotham A P, Madsen M, Kuemmeth F, Jespersen T S, Nygård J, Krogstrup P and Marcus C M 2016 Exponential protection of zero modes in Majorana islands *Nature* **531** 206
[15] Deng M-T, Vaitiekėnas S, Prada E, San-Jose P, Nygård J, Krogstrup P, Aguado R and Marcus C M 2018 Nonlocality of Majorana modes in hybrid nanowires *Phys. Rev.* B **98** 085125
[16] Vaitiekėnas S, Deng M-T, Nygård J, Krogstrup P and Marcus C M 2018 Effective g factor of subgap states in hybrid nanowires *Phys. Rev. Lett.* **121** 037703
[17] Nadj-Perge S, Drozdov I K, Li J, Chen H, Jeon S, Seo J, MacDonald A H, Bernevig B A and Yazdani A 2014 Observation of Majorana fermions in ferromagnetic atomic chains on a superconductor *Science* **346** 602
[18] Pawlak R, Kisiel M, Klinovaja J, Maier T, Kawai S, Glatzel T, Loss D and Meyer E 2016 Probing atomic structure and Majorana wave-functions in mono-atomic Fe-chains on superconducting Pb-surface *npj Quantum Inf.* **2** 16035
[19] Jeon S, Xie Y, Li J, Wang Z, Bernevig B A and Yazdani A 2017 Distinguishing a Majorana zero mode using spin-resolved measurements *Science* **358** 772
[20] Ruby M, Heinrich B W, Yang P, von Oppen F and Franke K J 2017 Exploring a proximity-coupled co chain on Pb(110) as a possible Majorana platform *Nano Lett.* **17** 4473
[21] Kim H, Palacio-Morales A, Posske T, Rózsa L, Palotás K, Szunyogh L, Thorwart M and Wiesendanger R 2018 Toward tailoring Majorana bound states in artificially constructed magnetic atom chains on elemental superconductors *Sci. Adv.* **4** eaar5251
[22] Deng M T, Yu C L, Huang G Y, Larsson M, Caroff P and Xu H Q 2012 Anomalous zero-bias conductance peak in a Nb–InSb nanowire-Nb hybrid device *Nano Lett.* **12** 6414
[23] Lin C-H, Sau J D and Das Sarma S 2012 Zero-bias conductance peak in Majorana wires made of semiconductor/superconductor hybrid structures *Phys. Rev.* B **86** 224511
[24] Prada E, San-Jose P and Aguado R 2012 Transport spectroscopy of *ns* nanowire junctions with Majorana fermions *Phys. Rev.* B **86** 180503
[25] Rainis D, Trifunovic L, Klinovaja J and Loss D 2013 Towards a realistic transport modeling in a superconducting nanowire with Majorana fermions *Phys. Rev.* B **87** 024515
[26] Pan H and Das Sarma S 2020 Physical mechanisms for zero-bias conductance peaks in Majorana nanowires *Phys. Rev. Res.* **2** 013377
[27] Kretinin A V, Shtrikman H, Goldhaber-Gordon D, Hanl M, Weichselbaum A, von Delft J, Costi T and Mahalu D 2011

Spin-$\frac{1}{2}$Kondo effect in an InAs nanowire quantum dot: unitary limit, conductance scaling, and Zeeman splitting *Phys. Rev.* B **84** 245316
[28] van der Wiel W G, De Franceschi S, Fujisawa T, Elzerman J M, Tarucha S and Kouwenhoven L P 2000 The Kondo effect in the unitary limit *Science* **289** 2105
[29] Lee E J H, Jiang X, Houzet M, Aguado R, Lieber C M and De Franceschi S 2014 Spin-resolved Andreev levels and parity crossings in hybrid superconductor–semiconductor nanostructures *Nat. Nanotechnol.* **9** 79
[30] Liu C-X, Sau J D, Stanescu T D and Das Sarma S 2017 Andreev bound states versus Majorana bound states in quantum dot-nanowire-superconductor hybrid structures: trivial versus topological zero-bias conductance peaks *Phys. Rev.* B **96** 075161
[31] Moore C, Stanescu T D and Tewari S Apr 2018 Two-terminal charge tunneling: disentangling Majorana zero modes from partially separated Andreev bound states in semiconductor–superconductor heterostructures *Phys. Rev.* B **97** 165302
[32] Moore C, Zeng C, Stanescu T D and Tewari S 2018 Quantized zero-bias conductance plateau in semiconductor-superconductor heterostructures without topological Majorana zero modes *Phys. Rev.* B **98** 155314
[33] Liu C-X, Sau J D and Das Sarma S 2018 Distinguishing topological Majorana bound states from trivial Andreev bound states: proposed tests through differential tunneling conductance spectroscopy *Phys. Rev.* B **97** 214502
[34] Liu D E and Baranger H U 2011 Detecting a Majorana-fermion zero mode using a quantum dot *Phys. Rev.* B **84** 201308
[35] Sasaki S, Tamura H, Akazaki T and Fujisawa T 2009 Fano–Kondo interplay in a side-coupled double quantum dot *Phys. Rev. Lett.* **103** 266806
[36] Žitko R 2010 Fano–Kondo effect in side-coupled double quantum dots at finite temperatures and the importance of two-stage Kondo screening *Phys. Rev.* B **81** 115316
[37] Ferreira I L, Orellana P A, Martins G B, Souza F M and Vernek E 2011 Capacitively coupled double quantum dot system in the Kondo regime *Phys. Rev.* B **84** 205320
[38] Wójcik K P and Weymann I 2014 Perfect spin polarization in T-shaped double quantum dots due to the spin-dependent Fano effect *Phys. Rev.* B **90** 115308
[39] Barański J and Domański T 2011 Fano-type interference in quantum dots coupled between metallic and superconducting leads *Phys. Rev.* B **84** 195424
[40] López R, Lee M, Serra L and Lim J S 2014 Thermoelectrical detection of Majorana states *Phys. Rev.* B **89** 205418
[41] Lee M, Lim J S and López R 2013 Kondo effect in a quantum dot side-coupled to a topological superconductor *Phys. Rev.* B **87** 241402
[42] Cao Y, Wang P, Xiong G, Gong M and Li X-Q 2012 Probing the existence and dynamics of Majorana fermion via transport through a quantum dot *Phys. Rev.* B **86** 115311
[43] Vernek E, Penteado P H, Seridonio A C and Egues J C 2014 Subtle leakage of a Majorana mode into a quantum dot *Phys. Rev.* B **89** 165314
[44] Gong W-J, Zhang S-F, Li Z-C, Yi G and Zheng Y-S 2014 Detection of a Majorana fermion zero mode by a T-shaped quantum-dot structure *Phys. Rev.* B **89** 245413
[45] Liu D E, Cheng M and Lutchyn R M 2015 Probing Majorana physics in quantum-dot shot-noise experiments *Phys. Rev.* B **91** 081405
[46] Stefański P 2015 Signatures of Majorana states in electron transport through a quantum dot coupled to topological wire *Acta Phys. Pol.* A **127** 198
[47] Li Z-Z, Lam C-H and You J Q 2015 Probing Majorana bound states via counting statistics of a single electron transistor *Sci. Rep.* **5** 11416
[48] Weymann I 2017 Spin Seebeck effect in quantum dot side-coupled to topological superconductor *J. Phys.: Condens. Matter.* **29** 095301
[49] Weymann I and Wójcik K P 2017 Transport properties of a hybrid Majorana wire-quantum dot system with ferromagnetic contacts *Phys. Rev.* B **95** 155427
[50] Andreev A F 1964 The thermal conductivity of the intermediate state in superconductors *J. Exp. Theor. Phys.* **19** 1228
[51] Chirla R and Moca C P Jul 2016 Fingerprints of Majorana fermions in spin-resolved subgap spectroscopy *Phys. Rev.* B **94** 045405
[52] Barański J, Kobiałka A and Domański T 2017 Spin-sensitive interference due to Majorana state on the interface between normal and superconducting leads *J. Phys.: Condens. Matter.* **29** 075603
[53] Górski G, Barański J, Weymann I and Domański T 2018 Interplay between correlations and majorana mode in proximitized quantum dot *Sci. Rep.* **8** 15717
[54] Maśka M M and Domański T 2017 Polarization of the Majorana quasiparticles in the Rashba chain *Sci. Rep.* **7** 16193
[55] Kogan A, Amasha S, Goldhaber-Gordon D, Granger G, Kastner M A and Shtrikman H 2004 Measurements of Kondo and spin splitting in single-electron transistors *Phys. Rev. Lett.* **93** 166602
[56] Amasha S, Gelfand I J, Kastner M A and Kogan A 2005 Kondo temperature dependence of the Kondo splitting in a single-electron transistor *Phys. Rev.* B **72** 045308
[57] Scott G D, Natelson D, Kirchner S and Muñoz E 2013 Transport characterization of Kondo-correlated single-molecule devices *Phys. Rev.* B **87** 241104
[58] García Corral A, van Zanten D M T, Franke K J, Courtois H, Florens S and Winkelmann C B 2020 Magnetic-field-induced transition in a quantum dot coupled to a superconductor *Phys. Rev. Res.* **2** 012065
[59] Franke K J, Schulze G and Pascual J I 2011 Competition of superconducting phenomena and Kondo screening at the nanoscale *Science* **332** 940
[60] Zhang H *et al* 2018 Quantized Majorana conductance *Nature* **556** 74
[61] Gül Ö *et al* 2018 Ballistic Majorana nanowire devices *Nat. Nanotechnol.* **13** 192
[62] Chevallier D, Szumniak P, Hoffman S, Loss D and Klinovaja J 2018 Topological phase detection in Rashba nanowires with a quantum dot *Phys. Rev.* B **97** 045404
[63] Barański J and Domański T 2013 In-gap states of a quantum dot coupled between a normal and a superconducting lead *J. Phys.: Condens. Matter.* **25** 435305
[64] Hwang S-Y, López R and Sánchez D 2016 Large thermoelectric power and figure of merit in a ferromagnetic–quantum dot–superconducting device *Phys. Rev.* B **94** 054506
[65] Domański T, Donabidowicz A and Wysokiński K I 2007 Influence of pair coherence on charge tunneling through a quantum dot connected to a superconducting lead *Phys. Rev.* B **76** 104514
[66] Žitko R, Soo Lim J, López R and Aguado R 2015 Shiba states and zero-bias anomalies in the hybrid normal-superconductor Anderson model *Phys. Rev.* B **91** 045441
[67] Suominen H J, Kjaergaard M, Hamilton A R, Shabani J, Palmstrøm C J, Marcus C M and Nichele F 2017 Zero-energy modes from coalescing Andreev states in a two-dimensional semiconductor–superconductor hybrid platform *Phys. Rev. Lett.* **119** 176805
[68] Tanaka Y, Kawakami N and Oguri A 2007 Numerical renormalization group approach to a quantum dot coupled to normal and superconducting leads *J. Phys. Soc. Japan* **76** 074701
[69] Górski G and Kucab K 2017 Irreducible Green's functions method for a quantum dot coupled to metallic and superconducting leads *Physica* E **89** 21–8

[70] Deacon R S, Tanaka Y, Oiwa A, Sakano R, Yoshida K, Shibata K, Hirakawa K and Tarucha S 2010 Kondo-enhanced Andreev transport in single self-assembled InAs quantum dots contacted with normal and superconducting leads *Phys. Rev.* B **81** 121308

[71] Deacon R S, Tanaka Y, Oiwa A, Sakano R, Yoshida K, Shibata K, Hirakawa K and Tarucha S 2010 Tunneling spectroscopy of Andreev energy levels in a quantum dot coupled to a superconductor *Phys. Rev. Lett.* **104** 076805

[72] Dirks T, Hughes T L, Lal S, Uchoa B, Chen Y-F, Chialvo C, Goldbart P M and Mason N 2011 Transport through Andreev bound states in a graphene quantum dot *Nat. Phys.* **7** 386

[73] Lee E J H, Jiang X, Žitko R, Aguado R, Lieber C M and De Franceschi S 2017 Scaling of subgap excitations in a superconductor-semiconductor nanowire quantum dot *Phys. Rev.* B **95** 180502

[74] Zienkiewicz T, Barański J, Górski G and Domański T 2020 Leakage of Majorana mode into correlated quantum dot nearby its singlet–doublet crossover *J. Phys.: Condens. Matter.* **32** 025302

[75] Prada E, Aguado R and San-Jose P 2017 Measuring Majorana nonlocality and spin structure with a quantum dot *Phys. Rev.* B **96** 085418

[76] Clarke D J 2017 Experimentally accessible topological quality factor for wires with zero energy modes *Phys. Rev.* B **96** 201109

[77] Ricco L S, Campo V L, Shelykh I A and Seridonio A C 2018 Majorana oscillations modulated by fano interference and degree of nonlocality in a topological superconducting–nanowire–quantum-dot system *Phys. Rev.* B **98** 075142

[78] Ricco L S, de Souza M, Figueira M S, Shelykh I A and Seridonio A C 2019 Spin-dependent zero-bias peak in a hybrid nanowire-quantum dot system: distinguishing isolated Majorana fermions from Andreev bound states *Phys. Rev.* B **99** 155159

[79] Schuray A, Weithofer L and Recher P 2017 Fano resonances in Majorana bound states-quantum dot hybrid systems *Phys. Rev.* B **96** 085417

[80] Hoffman S, Schrade C, Klinovaja J and Loss D 2016 Universal quantum computation with hybrid spin-Majorana qubits *Phys. Rev.* B **94** 045316

[81] Guessi L H, Dessotti F A, Marques Y, Ricco L S, Pereira G M, Menegasso P, de Souza M and Seridonio A C 2017 Encrypting Majorana fermion qubits as bound states in the continuum *Phys. Rev.* B **96** 041114

[82] Hoffman S, Chevallier D, Loss D and Klinovaja J 2017 Spin-dependent coupling between quantum dots and topological quantum wires *Phys. Rev.* B **96** 045440

[83] Górski G and Kucab K 2019 The spin-dependent coupling in the hybrid quantum dot-Majorana wire system *Phys. Status Solidi b* **256** 1800492